The Ginzburg interval in soft-mode phase transitions: consequences of the rigid unit mode picture

Peter Sollich†§, Volker Heine† and Martin T Dove‡

† Cavendish Laboratory, University of Cambridge, Madingley Road, Cambridge CB3 0HE, UK∥
‡ Mineral Physics Group, Department of Earth Sciences, University of Cambridge, Downing Street, Cambridge CB2 3EQ, UK¶

Abstract. In soft-mode structural phase transitions the Ginzburg temperature interval in which fluctuations and the interactions between them become important is often observed to be small on the scale of the transition temperature. We consider the size of the Ginzburg interval (GI) in framework and 'cogwheel' structures using the concept of 'rigid unit modes'. Such materials, as well as being very displacive, i.e. close to the soft-mode limit, have an extremely anisotropic phonon spectrum. Modelling these two properties with a suitable effective Hamiltonian for the degrees of freedom driving the transition we find that the GI can range from very small to large, depending on the balance between displaciveness and anisotropy. For the two perovskites $SrTiO_3$ and $LaAlO_3$ and the 'cogwheel' structure K_2SeO_4, we obtain values of the model parameters describing displaciveness and anisotropy from experimentally measured phonon dispersions and find, for the size of the GI, quantitative agreement with experiment. We also estimate typical values for the model parameters and the size of the GI for framework silicates, using quartz and cristobalite as examples. Finally, we use computer simulations to confirm the results of our theoretical analysis over a wider range of model parameters.

1. The Ginzburg interval in rigid unit mode systems

The purpose of this paper is to discuss the magnitude of the Ginzburg interval (GI), ΔT_G, in displacive structural phase transitions. We are concerned with materials that have strong anisotropies in the phonon spectra in the neighbourhood of unstable soft modes. These anisotropies can arise naturally, for example, in structures that consist of linkages of relatively rigid units, where the soft mode is one of the so-called 'rigid unit modes' that can propagate with no distortion of the units [1–4]. Rigid unit modes have been found to be particularly important in silicates, but we will point out later than similar anisotropies can arise in other systems. In this paper we will address the issue of the effect of the anisotropy of the phonon spectrum on the size of the GI.

Structural phase transitions in solids are traditionally described in terms of Landau free energies which contain the order parameter of the transition, Q, as a variational parameter. For example, minimization of the simple Landau free energy

$$F = \alpha(T - T_c)Q^2 + \beta Q^4 \tag{1}$$

§ Present address: Department of Physics, University of Edinburgh, Kings Buildings, Mayfield Road, Edinburgh EH9 3JZ, UK (e-mail address: P.Sollich@ed.ac.uk).
∥ e-mail address: tcmsec@phx.cam.ac.uk.
¶ e-mail address: martin@minp.esc.cam.ac.uk.

yields the 'classical' temperature dependence of the order parameter below the transition temperature T_c

$$Q(T) \propto (T_c - T)^{1/2} \tag{2}$$

which is obeyed quite well in many structural phase transitions over a wide temperature range [5].

It is known, however, that the expression (1) cannot be true arbitrarily close to the transition temperature. Within the GI long-wavelength fluctuations of the (local) order parameter increase without limit and become 'non-classical' in the sense that they can no longer be neglected or treated by a classical decoupling scheme such as mean field or renormalized phonon theory [6–8].

A traditional approach to determining the GI is to add terms of the form $\int dr \gamma (\nabla Q)^2$ to the Landau free energy (1) and to define the GI as the temperature region in which this augmented Landau free energy is no longer internally consistent [9]. (For a criticism of this method see, for example, [10].) The GI is thus expressed in terms of the phenomenological parameters α, T_c, β, γ of the augmented Landau free energy. Alternatively, one can obtain the GI starting from a description of the system in terms of an effective Hamiltonian, whose parameters reflect the microscopic mechanisms of the phase transition more directly than those of the Landau free energy. The materials with which we are concerned can be easily characterized in terms of an effective Hamiltonian, whereas the precise form of the corresponding Landau free energy is less clear; we shall therefore use a model effective Hamiltonian for our calculations of the GI.

We now describe the main features of the types of structures under consideration and the rigid unit mode characteristics of their phonon spectrum. We restrict ourselves to the essential features that will have to be contained in our model effective Hamiltonian and refer the reader to [3, 4, 11–14] for more details of the rigid unit mode model. Many materials contain or consist of rather rigid units such as tetrahedra, octahedra or (planar) triangles. In what we term 'framework' structures these form a continuous network by sharing corner atoms between adjacent units. Examples are many alumino-silicates containing joined AlO_4 and SiO_4 tetrahedra and perovskites containing XO_6 octahedra. The point about a framework structure is that the units are very stiff but are linked flexibly to each other at the corner atoms (although we note here that many perovskites cannot really be described in this way; however, we will continue to use the general perovskite structure as an example since it has the great advantage that it has a relatively simple structure). The following question then arises: if we treat the units as completely rigid, does the framework have any geometrically allowed phonon modes of motion in which the units only rotate and/or translate as rigid wholes? The answer is that such 'rigid unit modes' (RUMs) do indeed exist along special directions in the Brillouin zone [11, 14]. Clearly, in a real material, the RUMs will be phonons with a relatively low frequency with perhaps one of them resulting in a soft-mode phase transition as considered here, while all other phonons are typified by much higher frequencies because they necessarily involve distorting the rather stiff units.

We see therefore that the phonon spectra $\omega^2(k)$ of framework structures are very anisotropic, with 'valleys' in k-space where there are geometrically allowed RUMs. These valleys will make the dominating contributions to the fluctuations near T_c and determine the GI ΔT_G in our theory.

By way of example, consider the 'two-dimensional (2D) perovskite' structure shown in figure 1(*a*): a square lattice of octahedra representing the rigid units (and appearing as squares in the two-dimensional projection) linked via shared corner atoms. If one of these

(a)　　　　　　　　　(b)
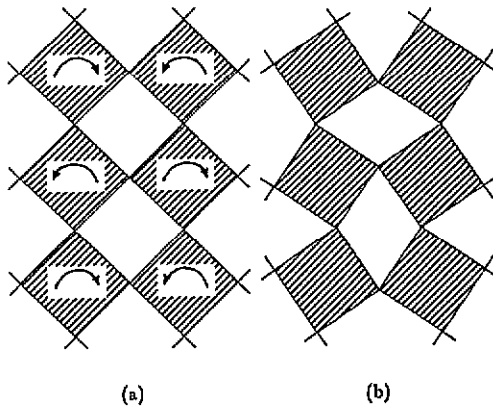
Figure 1. The 'two-dimensional perovskite' structure. Octahedra appear as squares in the projection; the links between neighbouring squares correspond to atoms shared between the octahedra in real perovskites. (*a*) Undistorted structure. (*b*) RUM displacement pattern. Notice how, by the opposite rotations of neighbouring octahedra indicated in (*a*), the shape of the octahedral units is preserved while none of the links between them is broken.

octahedra is rotated from its equilibrium position by an angle θ, it will try to rotate its nearest neighbours by an angle $-\theta$ in order to preserve its shape. In a 'knock-on effect', this leads to rotations of the next-nearest neighbours and so on, finally yielding the pattern of alternating rotations shown in figure 1(*b*). This displacement pattern is a RUM of 2D perovskite because it leaves the octahedral units undistorted. Since the rotation angles of neighbouring octahedra have opposite signs, the wavevector of this RUM lies at the corner of the Brillouin zone of the square lattice. It can be checked that 2D perovskite has no other non-trivial RUM and so we shall call the Brillouin zone corner RUM 'isolated'.

In general, however, framework structures can support a number of RUMs. To see how this happens, consider as an example 'three-dimensional (3D) perovskite', obtained by stacking layers of 2D perovskite on top of each other. A RUM for this structure can be constructed by rotating the octahedra in every plane according to the 2D perovskite RUM pattern. But as long as the corresponding rotation angles are sufficiently small, they can be chosen *independently* of each other without breaking the bonds between neighbouring octahedra in adjacent planes. Therefore, 3D perovskite has a line of RUMs in wavevector space, along the edge of the Brillouin zone corresponding to the direction perpendicular to the 2D perovskite layers. (Of course, there exist in fact three such RUM lines, since the octahedra can be rotated around each of the axes of the cubic lattice.) More complicated framework structures can be shown to have RUMs along planes or even across the whole of the Brillouin zone [11, 14].

While framework structures provide the clearest examples of RUMs, we believe that the situation is similar in other systems that contain distinct atoms or rigid molecular groups that do not share atoms. Examples involving 'cogwheel'-type motions are the A_2BX_4 salts such as K_2SeO_4, and biphenyl. In these materials one rigid unit can rotate easily only if neighbouring units also rotate in the manner of enmeshed cogwheels. The wrong rotations will bring into play the strong short-range repulsive forces between the units. Other systems involve atoms sliding across each other, maintaining a constant contact distance. Examples include the two ferroelastic materials HCN and Na_2CO_3 [4]. In the case of sliding systems, the anisotropy of force constants (analogous to the difference in framework structures between the stiffness of the units and the weak rotational interactions between

linked units) arises from the difference between the longitudinal (radial) and transverse (sliding) force constants between two atoms in contact. In all these examples the phonon spectrum will contain valleys in k-space containing the easy modes of distortion, with rather steep dispersion away from the soft directions, and our work will be directly relevant.

The structure of the paper is as follows. In section 2 we construct a suitable model of the phonon spectrum exhibiting the 'valleys' around the RUMs in k-space. This will be the main ingredient for the model effective Hamiltonian from which we calculate the GI. We consider two versions, one with a RUM line and one with a RUM plane, corresponding to a 'RUM dimensionality' $d_{RUM} = 1$ and 2, respectively. The model is characterized by two dimensionless parameters, s and ϵ. The 'displaciveness' s specifies how close the system is to the soft-mode limit at $s = 0$; the crossover from soft mode to order–disorder behaviour would occur around $s \approx 1$ in our model. We have shown elsewhere [12] that a RUM system will in general be near the soft-mode limit, i.e. have $s \ll 1$, because s is given more or less by the ratio of the weak forces between linked units, which drive the transition, to the large stiffness of the units. Other things being equal, a small s tends to give a small GI. The 'anisotropy' parameter ϵ measures the dispersion of $\omega^2(k)$ among the RUMs relative to the dispersion in the rest of the spectrum, so we expect $\epsilon \ll 1$. The larger ϵ, the less soft will be the RUMs away from the special point k_0 where the soft-mode transition occurs and hence the smaller the fluctuations and the GI will be. The third factor determining the size of the GI is the dimensionality of the RUM sector: a system with a plane of RUMs in k-space ($d_{RUM} = 2$) has larger fluctuations and a larger GI than a system with a RUM line ($d_{RUM} = 1$).

In section 3 we discuss the principles of how to calculate the GI from the model effective Hamiltonian for RUM systems, namely by determining the temperature region in which the best classical approximation breaks down. Our model treats only one coordinate per unit cell: the relevant rotation and/or translation of the rigid unit. The effect of all other optic and acoustic modes is swept up into the parameters of the model effective Hamiltonian. Since the system is in the soft-mode regime, the best classical approximation for analysing the effective Hamiltonian is the 'independent mode' approximation, from which the size of the GI is calculated in section 4. The results are presented and interpreted in terms of the displaciveness s and anisotropy ϵ, in particular for some limiting cases.

In section 5, we calculate the size of the GI quantitatively for the two perovskites $SrTiO_3$ and $LaAlO_3$ and the 'cogwheel structure' K_2SeO_4 and compare with experiment. We furthermore estimate typical values for the model parameters and the size of the GI for framework silicates, using quartz and cristobalite as examples.

Results of computer simulations we performed in order to confirm our theoretical analysis over a wider range of model parameters are reported in section 6. We conclude in section 7 with a brief summary of our results.

2. Model phonon spectrum for rigid unit mode systems

In this section we develop a model to represent the phonon spectrum relating to a soft-mode phase transition in a system with RUMs. It will be based on consideration of the perovskite structure but will be sufficiently general to be generic. We will use this phonon model as the quadratic part of our model effective Hamiltonian for RUM systems. Some of the (bare) phonons will be unstable, namely the soft mode and phonons near it; fourth-order terms in the effective Hamiltonian will stabilize the phonons at a high temperature and give a soft-mode phase transition at some T_c in the usual manner of the 'ϕ^4 model'.

The first point is to represent the stiffness of the units. As mentioned in section 1, all phonons except RUMs, by definition, involve some distortion of the rigid units. (We shall for convenience continue to refer to the units as 'rigid', meaning they have large but finite stiffness.) In figure 1(a) each square has five independent modes of distortion described by four force constants (two modes are degenerate); three-dimensional octahedra require even more parameters. It is easier, and for our purposes sufficient, to use the 'split-atom' approach [11, 14], considering the octahedra as totally rigid and instead treating each corner atom that links two adjacent octahedra as an elastic joint, i.e. as two halves of a 'split atom' with a harmonic spring between them. The finite stiffness of the octahedra is then modelled by the single force constant of this spring which tends to keep the corners of adjacent octahedra, i.e. the halves of the split atom, together.

In the 2D perovskite case, the potential energy of such a spring between neighbouring units i and j can be written as

$$\tfrac{1}{2}L(\phi_i + \phi_j)^2 \tag{3}$$

to lowest order in the rotation angles ϕ_i and ϕ_j. For $\phi_i = -\phi_j$ this expression vanishes, reflecting the fact that the units can rotate as rigid wholes without breaking the link between them (see figure 1(b)). For $\phi_i \neq -\phi_j$ we obtain a non-zero contribution due to the separation of the halves of the split corner atom which models the distortion that the octahedra would have to undergo were we to keep them linked via the 'un-split' corner atom. The coupling constant L in the split-atom model therefore corresponds to the stiffness of the octahedral units.

In order to have a force which drives the phase transition, we add a negative potential energy term

$$-\tfrac{1}{2}S(\phi_i - \phi_j)^2 \tag{4}$$

favouring the bending of bonds between neighbouring units. Clearly, this term needs to be countered by a positive higher-order term in order to make the system stable, but for the moment we only concern ourselves with the bare phonons and hence the quadratic contributions to the potential energy. We expect the (positive) force constant S describing forces *between* the octahedral units to be small (S) compared to the large (L) force constant which reflects the rigidity of the units [4, 12]:

$$S \ll L. \tag{5}$$

The total potential energy of our 2D perovskite model can now be written as

$$V_{2D} = \sum_{(i,j)} \tfrac{1}{2}L(\phi_i + \phi_j)^2 - \tfrac{1}{2}S(\phi_i - \phi_j)^2 \tag{6}$$

where the sum extends over all pairs of octahedra which are nearest neighbours. We transform to Fourier coordinates:

$$\phi(k) = \frac{1}{\sqrt{N}} \sum_{r_i} \phi(r_i) \exp(-ik \cdot r_i) \tag{7}$$

where N is the total number of octahedra, located at the lattice sites r_i. We obtain

$$V_{2D} = \frac{1}{2} \sum_k \bigl(-8S + J_{2D}(k)\bigr)\phi(k)\phi(-k) \tag{8}$$

with the sum running over all wavevectors in the two-dimensional Brillouin zone and

$$J_{2D}(k) = 2(L + S)(2 + \cos k_x a + \cos k_y a) \tag{9}$$

where a is the lattice parameter. Up to an unimportant mass scale, which we set to unity, we can read off the bare phonon spectrum of our model:

$$\omega_{2D}^2(k) = -8S + J_{2D}(k) \tag{10}$$

where the frequency of the Brillouin zone corner RUM is imaginary, $\omega^2(k = (\pi/a, \pi/a)) = -8S$, as required for a soft-mode phase transition in which this mode freezes.

If we now turn to 3D perovskite, all we need to do is to add up the contributions from the constituent 2D perovskite planes. In order to make the model a truly three-dimensional one, we add a coupling between neighbouring octahedra in adjacent planes of the form (3)

$$\tfrac{1}{2}S'(\phi_k + \phi_l)^2 \tag{11}$$

with a much smaller force constant S' obeying

$$S' \ll L \tag{12}$$

since the coupling between octahedra in adjacent planes arises not from distortion of the units but from bond-bending-type forces. We thus obtain for the potential energy of our 3D perovskite model

$$V_{3D} = \frac{1}{2}\sum_k (-8S + J_{3D}(k))\phi(k)\phi(-k) \tag{13}$$

with the sum now running over the three-dimensional Brillouin zone and

$$J_{3D}(k) = 2(L + S)(2 + \cos k_x a + \cos k_y a) + 2S'(1 + \cos k_z a). \tag{14}$$

In terms of the abbreviations

$$A = 8S \qquad J_r = 2S' \qquad J_n = 2(L + S) \tag{15}$$

for the modulus of the bare frequency of the most unstable RUM squared and the coupling constants determining the dispersion along RUM (suffix r) and non-RUM (suffix n) directions, the corresponding bare phonon spectrum $\omega_{3D}^2(k) = -8S + J_{3D}(k)$ is

$$\omega_{3D}^2(k) = -A + J_n(2 + \cos k_x a + \cos k_y a) + J_r(1 + \cos k_z a). \tag{16}$$

This is plotted schematically in figure 2 for k moving away from the most unstable RUM at $k_0 = (\pi/a, \pi/a, \pi/a)$ along the 'RUM direction', k_z, and along one of the non-RUM directions, k_x. We observe the following two characteristic features of the bare phonon spectrum.

(i) *Displaciveness.* The bare frequency squared of the most unstable RUM is small compared to the frequency squared of typical non-RUMs as a consequence of (5):

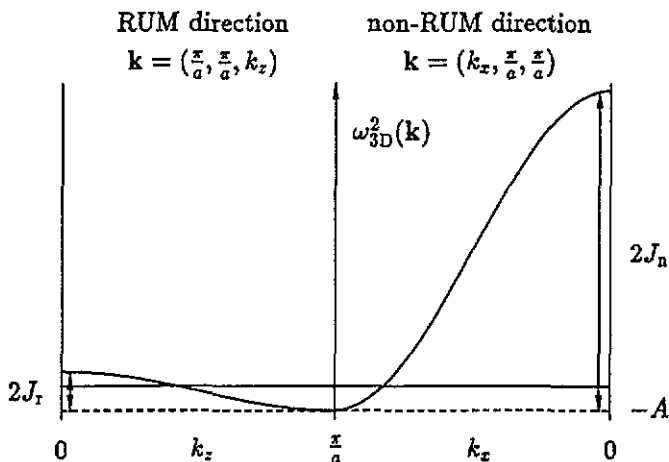$$s = \frac{A}{J_n} = \frac{8S}{L + S} \ll 1. \tag{17}$$

Figure 2. Schematic plot of the model bare phonon spectrum (16) for a RUM system, for k moving away from the most unstable RUM at $k_0 = (\pi/a, \pi/a, \pi/a)$ along a RUM direction, k_z, and along a non-RUM direction, k_x. The important features are displaciveness ($A \ll J_n$) and anisotropy ($J_r \ll J_n$).

We can say that the RUM line lies along 'the bottom of a steep valley' [4] in wavevector space or, equivalently, that the fraction of bare modes which are unstable is small.

(ii) *Anisotropy.* The dispersion along the direction of the RUM line is much smaller than away from it:

$$\epsilon = \frac{J_r}{J_n} = \frac{S'}{L+S} \ll 1 \tag{18}$$

as follows from (12). The smaller J_r (and hence ϵ) becomes, the larger the number of unstable bare modes.

Using the fact that the size of the GI decreases with the fraction of bare modes which are unstable (A P Levanjuk, private communication), we can qualitatively predict that the GI must become smaller as we increase the displaciveness (i.e. make s smaller) but larger as we increase the anisotropy (i.e. make ϵ smaller). The actual size of the GI will depend on the balance of these two factors, as pointed out in section 1.

It will sometimes be helpful to interpret our results in terms of two characteristic correlation length scales in RUM systems. As shown in the next section and in appendix 1, the parameter A gives not only the bare frequency squared of the most unstable RUM at the Brillouin zone corner k_0, but also the scale of the upwards renormalization of the phonon dispersion due to anharmonic effects, at temperatures well above or well below the phase transition. Using this, and expanding around k_0, we obtain for the typical renormalized (as opposed to bare) phonon dispersion around the lowest-frequency mode

$$\omega_{ren}^2(k) \approx +A + \tfrac{1}{2} J_n a^2 \big[(k_x - k_{0,x})^2 + (k_y - k_{0,y})^2 \big] + \tfrac{1}{2} J_r a^2 (k_z - k_{0,z})^2. \tag{19}$$

Disregarding all numerical factors, we read off that fluctuations along the (real-space) non-RUM directions x and y will typically be correlated over

$$\xi_n = (J_n/A)^{1/2} = s^{-1/2} \gg 1 \tag{20}$$

lattice units, whereas along the RUM direction z, correlations have a range of only

$$\xi_r = (J_r/A)^{1/2} = (\epsilon/s)^{1/2} = \epsilon^{1/2}\xi_n \ll \xi_n. \tag{21}$$

We stress here that we have defined ξ_n and ξ_r as temperature-independent quantities, quite unlike the temperature-dependent correlation lengths often used in, for example, discussions of critical phenomena. The quantities ξ_n and ξ_r can be thought of as 'prefactors' in the formulae for the corresponding temperature-dependent correlation lengths, setting the overall scale of correlations over a wide temperature range.

The inequalities for ξ_n and ξ_r given in (20) and (21) are derived from displaciveness (17) and anisotropy (18). For 3D perovskite, they can easily be understood geometrically. The value of ξ_n describes correlations between rotations of octahedra in the same '2D perovskite plane' which are strongly coupled due to the stiffness of the units and the knock-on effect discussed above. The much smaller value of ξ_r, on the other hand, reflects the fact that the octahedra in adjacent planes are only weakly coupled through bond-bending-type forces.

To summarize, the RUM picture has two crucial consequences. On the one hand, it leads to long-range correlations along directions where no RUMs exist, corresponding to a strong dispersion in k-space. On the other hand, correlations along RUM directions will be of rather short range, reflecting the flat dispersion along RUM lines or planes. Our main concern will be to analyse how the interplay of these two length scales affects the size of the GI.

3. Effective Hamiltonians and how to determine the size of the GI

We base our calculations of the GI on a model effective Hamiltonian which captures the essential features of RUM systems. We prefer starting from an effective Hamiltonian rather than a Landau free energy since the former contains in a more direct way information about the microscopic features of phase transitions in framework structures which the RUM model provides. Essentially, the effective Hamiltonian allows us to focus on the degrees of freedom most relevant to the transition. In the perovskite case, for example, the angles of rotation of the octahedra are the relevant degrees of freedom, whereas all other degrees of freedom can be considered irrelevant. Formally, an effective Hamiltonian can be defined with respect to an arbitrary set $\Psi = \{\psi_i\}$ of observables of a system as

$$\exp\big(-\beta H_{\text{eff}}(\Psi)\big) = \int d\Gamma \, \exp\big(-\beta H(\Gamma)\big)\delta\big(\Psi - \Psi(\Gamma)\big) \tag{22}$$

where H is the full Hamiltonian, Γ denotes a set of canonical phase space coordinates and $\beta = 1/k_B T$. From the relation between the effective Hamiltonian and the total free energy of the system

$$\exp(-\beta F) = \int d\Psi \exp\big(-\beta H_{\text{eff}}(\Psi)\big) \tag{23}$$

it can readily be seen that the effective Hamiltonian acts just like an ordinary Hamiltonian in generating the equilibrium distribution of the ψ_i. Due to the free energy contribution of the degrees of freedom not contained in Ψ, however, the effective Hamiltonian will in general depend on temperature. This temperature dependence will be 'smooth' (without non-analyticities at the transition temperature) if the set $\Psi = \{\psi_i\}$ contains all degrees of freedom whose fluctuations become non-classical, i.e. strongly interacting, near the phase transition.

How, then, do we determine the GI if we are given an effective Hamiltonian? We define the GI to be the temperature interval around a phase transition in which 'non-classical' behaviour occurs, in the sense that fluctuations *and* their interactions become important. Stated differently, inside the GI the behaviour of a system can no longer be described within a 'classical' approximation which decouples fluctuations and therefore effectively reduces the system to an assembly of simple non-interacting entities. Consequently, the GI can be determined by applying the most suitable classical approximation to a given effective Hamiltonian and checking where this approximation breaks down. We note three points.

Firstly, various classical approximation schemes might in general have to be tried out to establish which one is most suitable, i.e. optimal in approximating the actual behaviour of a system described by a given effective Hamiltonian. For the model effective Hamiltonian that we consider below, we can exploit results from the literature to avoid this complication.

Secondly, as the size of the GI depends on the precision of the classical approximation that we require, there is inevitably some arbitrariness in the calculation of it. In order to keep our discussion as quantitative as possible, beyond this inherent limitation, we keep throughout numerical constants that are often dismissed as 'of order unity' in discussions of the GI.

Thirdly, we follow the widely accepted assumption that the part of the GI extending above the transition temperature is approximately equal to the part below the transition, and we therefore only calculate the latter. Our calculations will yield the value of the order parameter at the lower boundary of the GI. We show in the next section how this quantity is related to the size of the GI on the temperature scale.

4. Model effective Hamiltonian for RUM systems and calculation of the GI

From our discussion in sections 1 and 2 it is clear that a model effective Hamiltonian for RUM systems must embody both displaciveness and anisotropy. The bare phonon dispersion (16) that we have read off from our model potential energy for 3D perovskite (13) already fulfills this requirement, and we take (13) as the quadratic part of our model effective Hamiltonian. For simplicity, however, we shift the most unstable RUM from the Brillouin zone corner to the zone centre in order to have an ordered (low-temperature) phase of the 'ferro' type. We also set $J = J_n$ and use definitions (17) and (18) to obtain

$$H_{\text{quadr}} = \frac{1}{2} \sum_k \left(-sJ + J(k)\right)\phi(k)\phi(-k) \tag{24}$$

with $J(k)$ given by

$$J(k) = J_{\text{line}}(k) = J(2 - \cos k_x a - \cos k_y a) + \epsilon J(1 - \cos k_z a). \tag{25}$$

This form of the bare phonon dispersion models systems with a RUM line as well as, for $\epsilon = 1$, systems with an isolated RUM. For the case of a RUM plane, all we need to do is to change the definition of $J(k)$ such that there are two RUM directions and only one non-RUM direction:

$$J(k) = J_{\text{plane}}(k) = \epsilon J(2 - \cos k_x a - \cos k_y a) + J(1 - \cos k_z a). \tag{26}$$

We now have to add an anharmonic part to our model effective Hamiltonian in order to make it stable. We choose a simple local fourth-order anharmonicity:

$$H_{\text{anharm}} = \frac{1}{4} \sum_i B\phi_i^4 = \frac{B}{4N} \sum_{k_1, k_2, k_3} \phi(k_1)\phi(k_2)\phi(k_3)\phi(-k_1 - k_2 - k_3) \tag{27}$$

and write our total model effective Hamiltonian, a 'ϕ^4-Hamiltonian', as

$$H = H_{\text{quadr}} + H_{\text{anharm}} = \frac{1}{2} \sum_k (-sJ + J(k))\phi(k)\phi(-k)$$

$$+ \frac{B}{4N} \sum_{k_1,k_2,k_3} \phi(k_1)\phi(k_2)\phi(k_3)\phi(-k_1 - k_2 - k_3) \tag{28}$$

with $J(k)$ given by (25) or (26), respectively. To be precise, we should add a kinetic energy term. This is however immaterial to our discussion and shall therefore be omitted.

Several comments are now in order. We think of the ϕ_i as generalizations of the octahedra rotation angles in our perovskite models, i.e. as local variables describing the rotations and/or translations of the units associated with the RUMs in the system under study. The $\phi(k)$ are the corresponding optic mode coordinates.

Furthermore, we have assumed the parameters B, J, s, ϵ to be temperature independent. This implies two assumptions. Firstly, that apart from the $\phi(k)$, no other degrees of freedom of the system undergo non-classical fluctuations near the phase transition, so that there are no non-analyticities in the temperature dependence of the model parameters. Secondly, we take the entropy contribution from these other 'irrelevant' degrees of freedom as non-essential for driving the transition, an assumption which is supported by calculations we have performed on quartz. Hence we assume our model parameters to be actually temperature independent, in contrast to other model effective Hamiltonians which often use a term like $a(T - T_0)$ instead of our $-sJ$, where T_0 sets a temperature scale at which entropy contributions from the degrees of freedom not explicitly retained in the effective Hamiltonian become important.

Finally, the model (28) is obviously too simple to describe the finer details of RUM systems. For our purposes, however, it captures the essential physics.

We now want to calculate the size of the GI in RUM systems as modelled by our effective Hamiltonian (28). As explained in the previous section, we do this by determining the validity of the best classical approximation. In our case this is the 'independent-mode' (IM) approximation in the sense of [8], since our systems are near the soft-mode limit. In fact Eisenriegler [15] found that the IM approximation becomes exact in the limit $s \to 0$. The results of the IM approximation, which provides a simple picture of the phase transition in terms of phonon softening, are summarized in appendix 1.

In order to establish the limits of validity of the IM approximation, we proceed as follows. We check the internal consistency of the IM approximation by determining how well it obeys the exact fluctuation-susceptibility relation given in appendix 2 in (A2.2). We derive the corresponding criterion for determining the lower boundary of the GI (which, incidentally, has the same functional form as the one derived by Bruce [8] within a different approach) in appendix 2. We denote by q the order parameter Q normalized to its value at zero temperature Q_0:

$$q(T) = Q(T)/Q_0 \tag{29}$$

and by q_G the value of this normalized order parameter at the lower boundary of the GI. The corresponding lower boundary temperature T_G of the GI is related to q_G via the IM equation of state (A1.6):

$$T_G = T_c^{\text{IM}}(1 - q_G^2)/c(q_G^2). \tag{30}$$

Here we have used the definition (A1.7) of the function $c(q^2)$, and the temperature T_c^{IM} is the lower stability limit of the disordered (high-temperature) phase within the IM approximation.

This is not quite the IM transition temperature itself because the IM approximation predicts (incorrectly) a slightly first-order transition at a temperature above T_c^{IM}. With this notation, our criterion is (see (A2.11) in appendix 2)

$$\frac{3}{4} \frac{T_G}{T_c^{IM}} \frac{J^{IM}}{sJ} \frac{1}{N} \sum_k \frac{1}{(q_G^2 + J(k)/2sJ)^2} \ll 1 \tag{31}$$

where J^{IM} is an effective coupling constant obtained by a suitable average over the $J(k)$ as defined in (A1.9).

The model effective Hamiltonian (28) is characterized by the four parameters B, J, s and ϵ. The effect of B and J can be absorbed into a rescaling of temperature and order parameter, and we are left with the two, by now familiar, dimensionless parameters s and ϵ characterizing the model. Since we are modelling displacive anisotropic systems, we expect both of these parameters to be small compared to unity, as spelled out in (17) and (18). Our calculations will yield q_G^2 as a function of these two parameters s and ϵ. This quantity can be related to the size of the GI on the temperature scale as follows. As mentioned above, we confine our attention to the part of the GI below the transition temperature, which can be expressed as

$$\Delta T_G = T_c - T_G \tag{32}$$

where T_c is the true transition temperature. If we normalize ΔT_G by T_c, we can write the inequality

$$\Delta T_G/T_c = 1 - T_G/T_c \leqslant q_G^2 \tag{33}$$

which can be used to convert between q_G^2 and ΔT_G. Equation (33) is a consequence of the inequality

$$q^2(T) \geqslant 1 - T/T_c \tag{34}$$

which follows from the fact that outside the GI the squared order parameter varies linearly with temperature (this can be verified from the IM equation of state (A1.6) [16]), but on further approaching T_c 'bends down' because the order parameter critical exponent of the ϕ^4 model is smaller than $1/2$ (see for example [8]).

For our actual calculations based on the criterion (31), we replace the inequality by an equality of the form

$$\frac{3}{4} \frac{T_G}{T_c^{IM}} \frac{J^{IM}}{sJ} \frac{1}{N} \sum_k \frac{1}{(q_G^2 + J(k)/2sJ)^2} = \kappa \tag{35}$$

where κ is a constant of order unity. For the derivations of the functional dependence of q_G on s and ϵ we use what seems the most natural choice, $\kappa = 1$; for comparison with experimental observations in section 5 and with the results of computer simulations in section 6, we also give the results for $\kappa = 0.5$ in order to see how variations in κ affect the value of q_G.

We rewrite (35) as

$$\frac{3}{4} \frac{T_G}{T_c^{IM}} f(\epsilon) \frac{1}{s} I(q_G^2; s, \epsilon) = \kappa \tag{36}$$

where

$$I(q_G^2; s, \epsilon) = \frac{1}{N} \sum_k \frac{1}{\left(q_G^2 + J(k)/2sJ\right)^2} \tag{37}$$

$$\left(f(\epsilon)\right)^{-1} = \frac{J}{J^{IM}} = \frac{1}{N} \sum_k \frac{J}{J(k)}. \tag{38}$$

The quantity $f(\epsilon)$ reflects within the IM approximation the effect of the anisotropy present in the system on the transition temperature. In fact, we have from (A1.9)

$$3k_B T_c^{IM} = f(\epsilon) J Q_0^2. \tag{39}$$

Before proceeding to a numerical calculation of $q_G^2(s, \epsilon)$ directly from (36), we want to analyse the behaviour of $q_G^2(s, \epsilon)$ in two limiting cases, for which we can calculate its functional form analytically to a good approximation. The dependence of $I(q_G^2; s, \epsilon)$ on q_G^2 and the parameters s and ϵ can be estimated as follows. One evaluates the sum in (37) by performing the corresponding integral over the Brillouin zone. Recognizing that the integrand has the form of a smooth high-frequency cutoff function, one can replace it to a first approximation by a sharp cutoff, setting the integrand to q_G^{-4} where $J(k)/2sJ \leqslant q_G^2$ and to zero otherwise. Writing $d_{RUM} = 1$ and 2 for a RUM line, one thus obtains

$$I \propto q_G^{-1} \epsilon^{-d_{RUM}/2} s^{3/2} \qquad q_G^2 \ll \epsilon/s \tag{40}$$

and

$$\begin{aligned} I &\propto q_G^{-2} s & q_G^2 \gg \epsilon/s & \qquad \text{for a RUM line} \\ I &\propto q_G^{-3} s^{1/2} & q_G^2 \gg \epsilon/s & \qquad \text{for a RUM plane.} \end{aligned} \tag{41}$$

The dependence of I on s and ϵ in (40) can be summed up by saying that each RUM direction contributes a factor of $(s/\epsilon)^{1/2} = \xi_r^{-1}$ and each non-RUM direction a factor $s^{1/2} = \xi_n^{-1}$, i.e. each direction contributes a factor proportional to the inverse of the correlation length in that direction. Equation (41) can be interpreted in the sense that the correlation length in the RUM directions is so short that it no longer appears in the result, so that the integral I effectively behaves as for a two- or one-dimensional system.

If we now consider the prefactor $f(\epsilon)$ in (36), defined in (38), we recognize that for $\epsilon = 0$, the integrand in (38) has a singularity at $k = 0$ which makes the integral divergent; f must therefore tend to zero as $\epsilon \to 0$. By considering the behaviour of the integrand in (38) near the singularities that arise as $\epsilon \to 0$ it can be shown that asymptotically

$$\begin{aligned} f(\epsilon) &\propto 1/|\ln \epsilon| & \text{for a RUM line} \\ f(\epsilon) &\propto \sqrt{\epsilon} & \text{for a RUM plane.} \end{aligned} \tag{42}$$

As yet, the behaviour of the factor T_G/T_c^{IM} in (36), which is related to q_G^2 by the IM equation of state (30), $T_G/T_c^{IM} = (1 - q_G^2)/c(q_G^2)$, has not been discussed. Following an argument by Bruce [8], one can assume that as long as q_G^2 is small, the approximation $T_G \approx T_c^{IM}$ is justified. In the limit of extreme anisotropy $\epsilon \to 0$, however, $T_c^{IM} \to 0$ from (39) and hence the factor T_G/T_c^{IM} can become large if the predicted value of q_G^2 lies in the

temperature region above T_c^{IM} where the IM still predicts the existence of a stable ordered phase. In this case it will be more convenient to consider the product

$$f(\epsilon)\frac{T_G}{T_c^{IM}} = \frac{3k_B T_G}{J Q_0^2} \tag{43}$$

because in the limit $\epsilon \to 0$, $T_G = T(q_G^2)$ is just given by the low (two- or one-dimensional) limit of the IM equation of state (30) and is no longer a function of ϵ.

Using the analytic estimates (40), (41) and (42), we now analyse the behaviour of q_G^2 in the two following limiting cases. First, consider the limit $\epsilon \to 0$ at constant s, which corresponds to a vanishing of the correlation length in the RUM directions, $\xi_r \to 0$. In this limit, one obtains an ensemble of uncoupled planes or lines (in real space) for a RUM line and plane, respectively. The dimensionality of the system is effectively reduced to two and one, respectively, and one expects a large Ginzburg interval. Indeed, from (36) we obtain that q_G^2 becomes large in this case since the divergence of the integral in (40) as $\epsilon \to 0$ is stronger than the approach of f to zero given by (42). This argument holds as long as ϵ is not too small so that the assumptions $T_G \approx T_c^{IM}$ and $q_G^2 \ll \epsilon/s$ are fulfilled. For values of ϵ considerably smaller than s, the second assumption is violated, and the integral I becomes independent of ϵ according to (41). Likewise, T_c^{IM} will tend to zero, leading to a violation of the first assumption; at the same time, however, the prefactor (43) becomes independent of ϵ as explained above. As $\epsilon \to 0$, q_G^2 must therefore eventually tend to a constant value, *which it should reach for values of ϵ well below s. Physically, this corresponds to the* fact that when $\epsilon \ll s$, the correlation length along the RUM directions becomes typically much smaller than one lattice unit, reducing the system to a collection of uncoupled two- *or one-dimensional subsystems, with the effect that the size of the GI reaches its limiting* lower-dimensional value and is no longer affected by a further increase in the anisotropy. To summarize, in the first limiting case ($\epsilon \to 0$, s = constant) the GI becomes independent of ϵ for $\epsilon \ll s$, both for a RUM *line* and a RUM *plane. This ϵ-independent limiting value* of the GI is fairly large even for very displacive systems, as the numerical results presented below will show.

The second limiting case of interest is $s \to 0, \epsilon \to 0$ with s/ϵ = constant. This corresponds to the limit of an infinite correlation length in the non-RUM directions ($\xi_n \to \infty$), which can be thought of as arising from completely rigid units, with a fixed correlation length along the RUM directions (ξ_r = constant). For a RUM *line*, one obtains from (36)

$$q_G^2 \propto f^2(\epsilon). \tag{44}$$

One can verify that this is indeed the solution of (36) using the fact that $f(\epsilon) \to 0$ as $\epsilon \to 0$ and hence $q_G^2 \to 0$. This implies from (40) that $I/s \propto q_G^{-1}(s/\epsilon)^{1/2} \propto q_G^{-1}$, and from (30) together with $c(0) = 1$ (see (A1.8)) that $T_G \to T_c^{IM}$, reducing the left-hand side of (36) to $f(\epsilon)/q_G$ = constant as required. For a RUM *plane*, on the other hand, one obtains from (36) that

$$q_G^2 \approx \text{constant}. \tag{45}$$

To verify this solution we observe that from either (40) or (41) one has $I/s \propto s^{-1/2}$ for given q_G^2 and constant s/ϵ and hence $f(\epsilon)I/s \propto (\epsilon/s)^{1/2}$ = constant from (42). Estimating the dependence of $c(q_G^2)$ on s and ϵ in a way analogous to the estimates for I given in (40) and (41), one can also show from (30) that $T_G/T_c^{IM} \approx$ constant; the left-hand side

of (36) is thus constant, as required. For the second limiting case ($s \to 0, \epsilon \to 0$ with s/ϵ = constant) we have thus found that the GI tends to zero for the case of a RUM *line*, but approaches a non-zero value in systems with a RUM *plane*. This means that in the limit of an infinite correlation length along the non-RUM directions, the short-range correlations introduced by the presence of multiple RUMs keep the GI finite for the case of a RUM plane, where the strongest fluctuations occur on a two-dimensional sector of wavevector space, whereas their effect is suppressed and the system behaves entirely classically for a RUM line, where fluctuations are confined to a one-dimensional set of wavevectors. This agrees with the general statement that the effect of fluctuations depends strongly on the dimensionality of the phase space region where they occur.
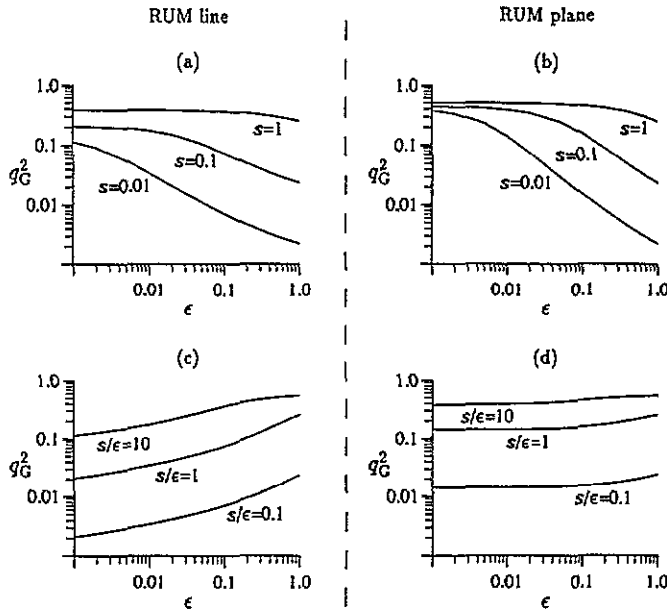

Figure 3. Size of the Ginzburg interval in RUM systems as a function of displaciveness s and anisotropy ϵ. Shown is the value of q_G^2, the square of the normalized order parameter at the lower boundary of the GI, as a function of ϵ, with s determined as follows. (*a*) and (*b*): Fixed s, corresponding to a fixed correlation length ξ_n along the non-RUM directions, for systems with a RUM line and plane respectively. (*c*) and (*d*): Fixed s/ϵ, corresponding to a fixed correlation length ξ_r along the RUM directions, again for a RUM line and plane respectively. Equation (33) can be used to convert from q_G^2 to the size ΔT_G of the GI on the temperature scale.

We now present the results of numerical calculations of $q_G^2(s, \epsilon)$. These results were obtained by directly solving (36) for q_G^2 by numerical integration and hence do not involve any of the approximations made above in the analytic treatment of the limiting cases. We remind readers more used to seeing the size of the GI expressed in terms of a temperature interval of the relation (33), which can be used to convert from the order parameter (q_G^2) to the temperature (ΔT_G) scale. In figures 3(*a*) and 3(*b*) we show for the case of a RUM line and plane, respectively, the dependence of q_G^2 on ϵ for fixed values of s. This form of presentation confirms the results of our analysis of the first limiting case above ($\epsilon \to 0$ at s = constant). The initial increase of q_G^2 with decreasing ϵ can clearly be seen, and q_G^2 attains a constant value for $\epsilon \ll s$. This limiting value depends only weakly on s and is,

even for a very displacive system ($s = 0.01$), sufficiently large to be detected experimentally in a corresponding real system. In figures 3(c) and 3(d) we have plotted, again for the case of a RUM line and plane respectively, the dependence of q_G^2 on ϵ for fixed values of s/ϵ. We can thus confirm our results obtained above for the second limiting case $s \to 0, \epsilon \to 0$ at $s/\epsilon = $ constant. For a RUM line, $q_G^2 \to 0$ as $\epsilon \to 0$, whereas for a RUM plane, q_G^2 tends to a constant in the same limit.

Altogether, our results show that the GI in RUM systems is not necessarily always small and can, in fact, be large. The application of our theory to real materials in the next section will show, however, that typical 'real-world' values for the parameters s and ϵ nevertheless yield relatively small GI, of the order of $\Delta T_G/T_c \leqslant q_G^2 \approx 0.1$ or less.

5. Application to real materials

In this section, we make quantitative comparisons between the theoretical results of section 4 for the size of the GI and experimental observations on real materials. We consider the two perovskites SrTiO$_3$ and LaAlO$_3$ (which have a framework structure of octahedra joined by shared oxygen atoms), and the 'cogwheel' structure K$_2$SeO$_4$. We also give qualitative estimates for quartz and cristobalite, which are examples of framework silicates.

The choice of the three materials for the quantitative calculations was based on the availability of experimental data in two respects. It had to be possible to determine the GI from the measured temperature dependence of the order parameter or the specific heat, and data on the temperature dependence of the soft mode and the dispersion in its environment in k-space had to be available in order to allow a meaningful input of data into our model.

The perovskites SrTiO$_3$ and LaAlO$_3$ both undergo displacive phase transitions, at temperatures around 105 K and 800 K, respectively [17]. In both cases, the atomic displacement pattern in the ordered phase corresponds to rotations of the perovskite-typical octahedra (TiO$_6$ and AlO$_6$, respectively) with opposite signs in neighbouring unit cells, corresponding to a soft mode at the corner point R of the Brillouin zone. In SrTiO$_3$, the rotation is around one of the cubic axes, leading to a tetragonal structure in the low-temperature phase, whereas it is around a body diagonal of the cubic unit cell in LaAlO$_3$, resulting in a trigonal symmetry of the ordered phase.

In the application to real materials, the field ϕ in our model effective Hamiltonian corresponds to the specific combination of atomic displacements that occurs in each unit cell during the phase transition. Assuming that the atomic displacement patterns of the Fourier modes $\phi(k)$ correspond to actual phonons occurring in the real material, we will model the dispersion of the $\phi(k)$ on that of the corresponding real phonons.

As explained in section 4, we only need to know the parameters s and ϵ of our model effective Hamiltonian (28), i.e. the values of $A = sJ$, J and ϵ, in order to determine the size of the GI relative to the transition temperature.

For SrTiO$_3$, this quadratic part was obtained from experimental data as follows. The dispersion of the three phonon branches containing the threefold degenerate soft mode at the R point was taken from [18, 19] in the form of the dynamical matrix

$$R_{ij}(k) = [a(T) + \lambda(k^2 + f k_i^2)]\delta_{ij} + \lambda h k_i k_j (1 - \delta_{ij}) \tag{46}$$

with

$$\lambda = 216 \pm 20 \text{ (THz Å)}^2 \qquad f = -0.97 \pm 0.01 \qquad h = 0.19 \pm 0.04. \tag{47}$$

Neglecting the off-diagonal elements, which give a small relative second-order frequency shift of the order of $h^2/|f| \approx 0.04$, one obtains, with a value for the lattice constant of SrTiO$_3$ of $a = 3.9$ Å [20], the model parameter values

$$J = 2\lambda/a^2 \approx 28 \text{ THz}^2 \qquad \epsilon = 1 + f = 0.03 \pm 0.01. \qquad (48)$$

The parameter $A = sJ$ was obtained from the measured soft-mode frequency above T_c as follows. The measurements by Cowley and co-workers [21] yield a linear temperature dependence of the soft-mode frequency squared above T_c, which extrapolates to approximately -1.2 THz^2 at zero temperature. Hence A was determined from the requirement that, for the given values of J and ϵ, the soft-mode frequency predicted by the IM approximation extrapolate to the same value at $T = 0$, with the result $A = 2.0 \text{ THz}^2$. The displaciveness parameter s is thus $s \approx 2/28 \approx 0.07$.

We now obtain with this input from the IM criterion (36) the value of q_G^2, the square of the order parameter (normalized to its value at zero temperature) at the lower boundary of the GI. Inserting the extreme values of the anisotropy parameter, $\epsilon = 0.02$ and 0.04, and choosing $\kappa = 1$ and 0.5 we find

$$q_G^2 = \begin{cases} 0.09\text{--}0.12 & \kappa = 1 \\ 0.25\text{--}0.29 & \kappa = 0.5. \end{cases} \qquad (49)$$

In view of the rather pronounced dependence of these results on κ, no detailed analysis of the effect of the uncertainties in the values of A and J was carried out.

The above theoretical results can now be compared to the experimental observations by Mueller and Berlinger [17]. They found a linear dependence of Q^2 on temperature for $0.7 \leqslant T/T_c \leqslant 0.9$ which extrapolates to zero at $T \approx 1.05 \, T_c$, whereas for $0.9 \leqslant T/T_c \leqslant 1$, $Q^2(T)$ deviates from a straight line; the authors conclude that the GI is of the order $0.1T_c$. The above results (49) agree quantitatively with this observation. The approximately linear dependence of $q^2(T)$ for $0.7 \leqslant T/T_c^{IM} \leqslant 0.9$ predicted by the IM approximation for our model extrapolates to zero at $\approx 1.2 \, T_c^{IM}$, yielding $T_c \approx 1.2 \, T_c^{IM}/1.05 \approx 1.14 \, T_c^{IM}$ as an estimate for the relation between the real transition temperature and the one predicted by the IM approximation; the temperatures T_G corresponding to the average values $q_G^2 = 0.27$ and 0.105 taken from (49) for $\kappa = 0.5$ and $\kappa = 1$, respectively, can be calculated from the IM equation of state (A1.6) to be $0.93T_c^{IM} \approx 0.81T_c$ and $1.04T_c^{IM} \approx 0.91T_c$, bracketing the experimental value of $0.9T_c$ for the lower boundary temperature T_G of the GI. Note that the inequality (33), $\Delta T_G/T_c \leqslant q_G^2$, is satisfied since for both values of κ

$$\frac{\Delta T_G}{T_c} = \frac{T_c - T_G}{T_c} = 1 - \frac{T_G}{T_c} \approx \begin{cases} 1 - 0.81 = 0.19 \\ 1 - 0.91 = 0.09 \end{cases} \leqslant \begin{cases} 0.27 \\ 0.105 \end{cases} = q_G^2 \qquad (50)$$

and that q_G^2 provides a fairly tight bound on $\Delta T_G/T_c$.

We note that the interpretation by Mueller and Berlinger [17] of the experimentally observed size of the GI is different from ours. They use the traditional Ginzburg criterion for isotropic systems to find a zero-temperature correlation length in the sense of [6, 7] of $\xi_0 = 1.36$ nm, i.e. in lattice units $\xi_0/a \approx 3.3$, and interpret this as a short-range correlation between octahedra at equivalent positions in the ordered phase which has a lattice constant of $2a$.

Ginzburg [22], on the other hand, estimated a zero-temperature correlation length ξ_0 greater than five lattice units for SrTiO$_3$ and concluded, again from the isotropic Ginzburg criterion, that the GI should be experimentally unobservable.

Our interpretation takes account of the strong anisotropy caused by the existence of RUM lines. In the direction perpendicular to the RUM lines we have a correlation length of approximately $\xi_n = s^{-1/2} \approx 4.8$ lattice units, in agreement with Ginzburg's estimate and in contradiction to the Mueller and Berlinger result of short-range correlations. Along the direction of a RUM line, however, the correlation length is approximately given by $\xi_r = \epsilon^{1/2}\xi_n$, hence smaller by a factor of $\epsilon^{1/2} \approx 0.14$–$0.2$ and thus of the order of one lattice unit. As our calculation shows, the GI is determined by both these correlation lengths and the inherent anisotropy of the correlations cannot be neglected.

We now turn to the case of LaAlO$_3$. In this material, the displacement pattern in the ordered phase is a rotation of AlO$_6$ octahedra about a body diagonal of the cubic lattice, corresponding to a linear combination with equal weights of rotations around the cubic axes x, y and z. The bare phonon spectrum, taken as a whole, is again very anisotropic with RUM lines in the k_x, k_y and k_z directions along the edges of the Brillouin zone. However, these RUMs involve rotations about the x, y and z axes respectively, and thus do not correspond to the order parameter of the actual transition. Our one-component model (28) of section 6 only involves fluctuations of the latter, with other phonons being irrelevant. Since the observed order parameter contains all three rotations equally, it would seem that we need to take an isotropic model. The lack of anisotropy in the fluctuations has been observed experimentally by Kjems and co-workers [23] who have already alluded to a similar explanation.

From the data of [23] the model parameters $A = sJ$, J and ϵ were obtained in the same way as for the case of SrTiO$_3$ above. The soft-mode branch dispersion around the R point is observed to be $\omega^2 = \lambda k^2$ with $\lambda = 2000\,\text{meV\,\AA}^2$ for all three soft-mode branches, yielding $\epsilon = 1$ and, with the lattice constant $a = 3.79\,\text{\AA}$ [24], $J = 2\lambda/a^2 \approx 280\,\text{meV}^2$. The observed linear temperature dependence of the square of the soft-mode frequency (denoted by ω_∞^2 in [23]) above the transition extrapolates to approximately $-57\,\text{meV}^2$ at $T = 0$, and the corresponding value of the parameter A was found to be $A \approx 95\,\text{meV}^2$, leading to $s \approx 95/280 \approx 0.34$.

The calculated values of q_G^2 for these model parameters are, again for $\kappa = 1$ and $\kappa = 0.5$:

$$q_G^2 = \begin{cases} 0.09 & \kappa = 1 \\ 0.28 & \kappa = 0.5. \end{cases} \tag{51}$$

The close similarity of the q_G^2 values obtained for SrTiO$_3$ and LaAlO$_3$ agree well with the experimental observation by Mueller and Berlinger [17], who found that the dependence of the order parameter on temperature (measured on the scale of the transition temperature) in the two materials—and hence the size of the GI relative to T_c—was strikingly similar.

While our considerations cannot, of course, explain *why* the parameters for the dispersion in the two perovskites we have considered conspire with differing degrees of anisotropy to give the same size of the GI, the above comparison shows that our calculations take correct account of the influence of anisotropies on the size of the GI and that the results agree well with experiment.

We have already shown in section 1 that the idea of RUMs can be extended to cogwheel structures in which the rotations of adjacent rather rigid units are coupled through steric hindrance between them. The A$_2$BX$_4$ family of compounds provide a good example [25]. Many of them undergo phase transitions in which all the BX$_4$ units (which present a triangular profile in the yz plane) in the same yz layer rotate together in the same sense [25].

This rotation about the x axis is the major component in the order parameter of the incommensurate phase transition [25]. For K$_2$SeO$_4$, the observed [26] and calculated [25, 27] phonon spectra are very anisotropic, with an anisotropy ratio nearly as great as in SrTiO$_3$

above. Thus we can apply the RUM phonon model of section 2, in particular equation (25), for a RUM line describing softish phonons along the k_x axis with hard phonons everywhere else.

We can make estimates of the quantities $A = sJ$, J and ϵ for K_2SeO_4 as follows. We note from [25] that the overall width of the phonon spectrum from Raman spectroscopy and computer simulations is $162\,cm^{-1}$, excluding internal optic modes of the BX_4 units, which are treated as rigid. This width includes optic vibrations of the K^+ ions against the SeO_4^{2-} ions and we therefore reduce our width rather arbitrarily to $125\,cm^{-1}$, giving $2J = 15\,625\,cm^{-2}$. For the soft-mode RUM band we adopt the revised computer model of [27] and on the positive ω^2 side we include the non-acoustic part near $k = 0$, giving a total RUM bandwidth from $-31\,cm^{-1}$ to $+33\,cm^{-1}$, i.e. of $2\epsilon J = (31^2+33^2)\,cm^{-2} = 2050\,cm^{-2}$. The value of $A = sJ$ is the negative ω^2 of the bare soft mode, which from the phonon model in [28] is $A = 960\,cm^{-2}$. This seems more reliable than the value $A = 1600\,cm^{-2}$ of the earlier phonon model [25]. The value $A = 960\,cm^{-2}$ is also reasonable because it is somewhat larger (as it should be) than the extrapolation of the observed ω^2 from above T_c down to $T = 0$ which gives $|\omega^2(\text{extrapolated})| = 630\,cm^{-2}$ [25]. These estimates are probably as good as can currently be made; in particular, we note that the RUM branch does not soften uniformly as a whole [28], unlike our model. With these reservations therefore we have $s \approx 0.12$ and $\epsilon \approx 0.13$. From figure 3(c) we can then simply read off $q_G^2(\kappa = 1) = 0.08$ and, with the transition temperature $T_c = 130\,K$, a Ginzburg interval $\Delta T_G \leqslant q_G^2 T_c \approx 10\,K$. The specific heat data from [29] gives $\Delta T_G \approx 5$–$10\,K$, which we consider to be reasonable agreement.

We end this section by qualitatively considering quartz and cristobalite. Our motivation is that they can be taken as representative of silicate framework structures with tetrahedral SiO_4 units, for which the RUM model was originally developed. Both quartz (see for example [30]) and cristobalite [31] have a first-order transition (whereas our model gives a second-order transition), and the square of the order parameter does not vary linearly with temperature outside the GI as our model predicts. Hence no direct comparison of the theoretical results given below with experiment is possible. We may simply take our values of s and ϵ as well as the calculated $\Delta T_G/T_c \leqslant q_G^2$ as typical of what might be expected in tetrahedral framework silicates. Due to the lack of experimental information, we base our theoretical estimates on computed phonon spectra.

We have calculated phonon spectra for the β phases of quartz and cristobalite using the interatomic potentials of [32]. These required the use of the ideal structures, which are probably not fully realized in the real situations owing to the apparently shortened Si–O bonds. Accordingly we have also incorporated recent inelastic neutron scattering data for quartz [30]. In the case of quartz we calculate from the bare frequency at $k = 0$ a value of $A = sJ = 6\,THz^2$. The experimental value is of the order of $1.5\,THz^2$, found by extrapolating the data of [30] to $T = 0\,K$. The RUM bands extend to 0, 2.5 and $4\,THz^2$ along the RUM lines in the Δ, Σ and Λ directions respectively. If we take an average of these values, and use the experimental value for A, we obtain an estimate for $2\epsilon J = 3.5\,THz^2$, giving a value for the ratio of s/ϵ of order unity. We estimate a value for $2J$ as given by the range of phonon frequencies excluding the modes involving Si–O stretch motions, which gives $2J = 130\,THz^2$. Thus we have $s \simeq \epsilon \simeq 0.025$. We stress that these are only rough estimates, but we believe that they will be appropriate for other silicates such as cristobalite.

Quartz is an example of a system with lines of RUMs. Using our estimates for s and ϵ we read from figures 3(a) and (c) the result $\Delta T_G/T_c \leqslant q_G^2 \approx 0.045$, which with $T_c = 858\,K$ gives a value for ΔT_G of about $40\,K$.

Cristobalite is an example of a system with planes of RUMs [4, 14, 33]. From figures 3(b) and 3(d) we note that for a constant value of s/ϵ the size of q_G is fairly insensitive to the value of s (or equivalently to ϵ). Using the same values of s and ϵ as we used for quartz, we obtain $q_G^2 = \Delta T_G/T_c \approx 0.1$. The transition in cristobalite is strongly first order, so it is not clear whether the value for T_c should be the actual transition temperature (530 K) or the temperature that appears in the quadratic term of the Landau free energy (230 K), i.e. the point towards which the order parameter susceptibility will diverge. These give values for ΔT_G of about 50 K and 25 K respectively, but in any case it should be noted that the discontinuity in the order parameter at the transition is larger than our estimate of q_G.

The sizes of the GI we have estimated for quartz and cristobalite are larger than we had initially expected [3, 4]. Our estimates, though, are subject to error, perhaps as large as a factor of 2–3, but probably not large enough to allow the size of the GI to become vanishingly small. However, large values for the GI might suggest that the first-order transitions in these systems could be valid examples of fluctuation-driven first-order transitions (I P Swainson, private communication).

It is worth commenting that in all the materials discussed above we have s of the order of 0.1. This seems to be typical of the ratio of Coulomb forces which are active in RUMs, to the atomic hard-core repulsions which come into play in non-RUMs. The value of s can be related to the coefficient α in the Landau free energy (1) by a slight reworking of renormalized phonon theory (V Heine, unpublished) and it can be checked that $s \approx 0.1$ does indeed correspond to the values of α typically found in soft-mode phase transitions (R Currat, private communication).

6. Comparison with computer experiments

In order to confirm our results from section 4 for the size of the Ginzburg interval in RUM systems over a wider range of model parameters than that covered by real materials, computer simulations of the system described by the effective Hamiltonian (28) were carried out in the displacive anisotropic regime ($s, \epsilon \ll 1$) relevant for the description of RUM systems.

From the 'experimental' results of these simulations, the GI was determined by comparing the observed temperature dependence of the order parameter with the predictions of the IM approximation and identifying the order parameter value at which the agreement became unsatisfactory. Given that it is expected that the computer experiments will begin to see the finite sample size at temperatures close to the transition temperature, the agreement between the simulations and the results of the IM model will provide an upper bound on the value of the GI rather than the actual size of the GI.

The ϕ^4 Hamiltonian (28) has been used extensively as a standard model for phase transitions and has, of course, been investigated by computer simulations before. In particular, Schneider and Stoll [34, 35] have performed extensive studies of the isotropic ϕ^4 model in two and three dimensions, focusing on critical behaviour and dynamical aspects. Kerr and Bishop [36] have studied an extremely anisotropic two-dimensional model, again with an emphasis on the model dynamics. Padlewski and co-workers [37] have studied the crossover from order–disorder to displacive behaviour in the isotropic ϕ^4 model.

The simulations were carried out on the AMT distributed array processor (DAP) in Cambridge, which has 4096 processors. The simulated sample was a $16 \times 16 \times 16$ cubic lattice, on which periodic boundary conditions were imposed in order to eliminate surface effects as far as possible. A microcanonical ensemble was used; thus the equations of motion

for the fields ϕ_i were just the Newtonian equations of motion that result when the effective Hamiltonian (28) is treated as a classical potential energy. The numerical integration of these equations was performed using the leap-frog Verlet algorithm, as described in [38, 39].

Two series of model parameters were studied, separately for the case of a RUM line and plane:

$$(s, \epsilon) = (0.05, 1) \qquad (0.05, 0.1) \qquad (0.05, 0.01)$$
$$(s, \epsilon) = (5, 1) \qquad (0.5, 0.1) \qquad (0.05, 0.01). \tag{52}$$

These two series correspond to the approach to the two limiting cases discussed in section 6. In the first series, s = constant and ϵ decreases, implying that the correlation length ξ_r along the RUM directions decreases towards zero; in the second series, s/ϵ = constant and $s \to 0$, corresponding to the case where the correlation length ξ_n along the non-RUM directions becomes large. We remark that the first parameter set ($s = 5, \epsilon = 1$) in the second series of (52) actually corresponds to a non-displacive isotropic system, which we do not expect to be a good model for real RUM systems and for which our analysis in terms of the IM as the best classical approximation is not strictly valid. We nevertheless included this case to make the overall trend in the second parameter series more obvious.

The results for the order parameter as observed in our simulations are shown in figures 4 and 5, together with the predictions of the IM approximation and the GI as calculated from (36) for $\kappa = 0.5$ and 1. The first series of model parameters is shown in figure 4, and the second one in figure 5. Note that in the temperature region where the IM equation of state (A1.6) has two solutions for $q^2(T)$, the lower branch is unstable, and the upper branch is only metastable above the first-order transition predicted by the IM approximation. Also note that we worked with units in which $J = Q_0^2 = 1$ and $k_B = 1$.

It can clearly be seen that the agreement between the computer experiments and the IM predictions is satisfactory outside the calculated GI, especially when it is taken into account that no fitting parameters or correction factors for finite-size effects have been introduced. Inside the calculated GI, on the other hand, deviations between the IM predictions and the computer experiments occur as expected.

We further exploited the results of the computer experiments in order to see how well the size of the GI, determined from the temperature dependence of the order parameter, correlates with what one would obtain by analysing other observables of the system. As these other observables we chose the squared renormalized phonon frequencies at five specific wavevectors, which were measured as a function of temperature and compared to the best classical, i.e. IM approximation, predictions. The results, which we do not present in detail here, show that indeed the size of the GI determined from the renormalized frequencies correlates well, at least qualitatively, with that determined from the order parameter.

In conclusion, it can be said that the computer experiments support the theoretical analysis of section 4 for the size of the GI in systems described by the effective Hamiltonian (28) which we used to model the characteristic features (displaciveness and anisotropy) of RUM systems.

Although the simulations presented here were aimed at studying a different region of the parameter space of the ϕ^4 model than that investigated by Padlewski and co-workers [37], the results have some bearing on their conclusion that the ϕ^4 model exhibits classical behaviour only in the double limit of displaciveness and long interaction range. In fact, the results for the most displacive isotropic system studied above ($s = 0.05, \epsilon = 1$; see the top graph of figure 4) show that classical behaviour is obtained for pure nearest-neighbour interactions if the system is displacive enough. The discrepancy with the conclusion of
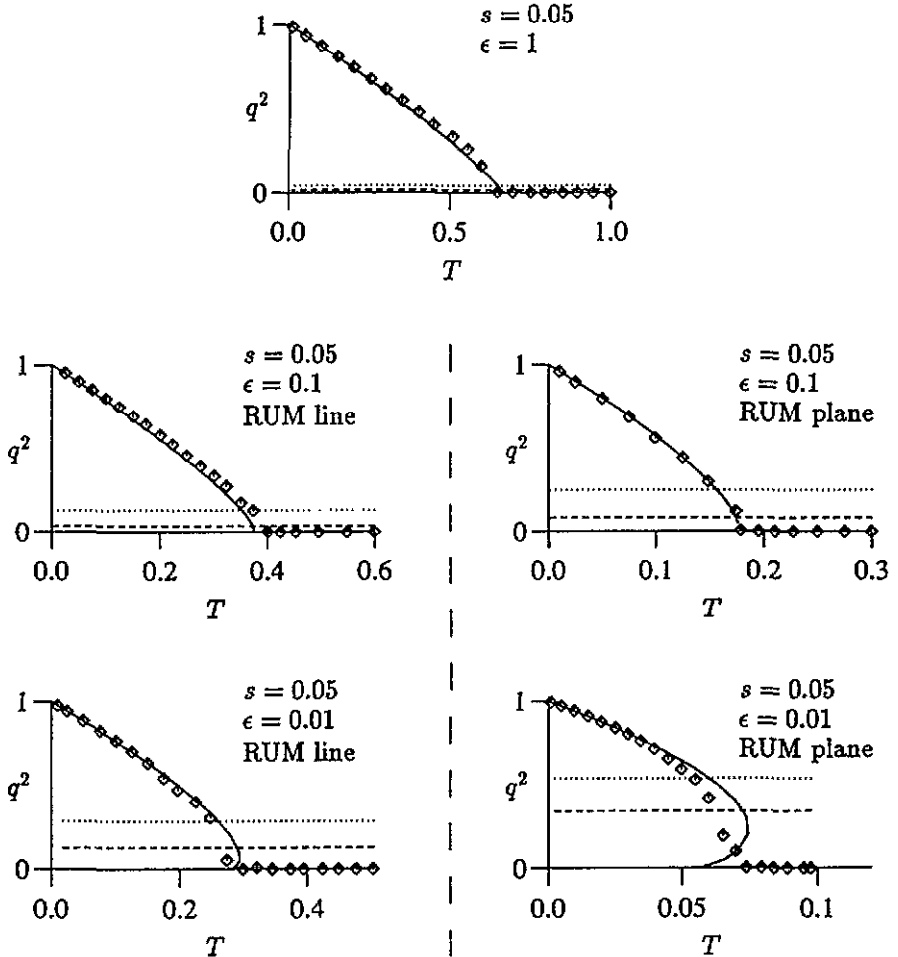
Figure 4. Square of the normalized order parameter q^2 as a function of temperature T, as measured in computer experiments (diamonds) and as predicted by the IM approximation (full curves). The GI can be read off as the temperature interval where large discrepancies occur. The horizontal dotted and broken lines indicate the theoretical values q_G^2 for q^2 on the lower boundary of the GI as calculated from (36) for $\kappa = 0.5$ and 1 respectively. Shown, from top to bottom, are the first parameter series from (52), both for a RUM line and a RUM plane as indicated. For $\epsilon = 1$, one has only an isolated RUM.

Padlewski and co-workers can be attributed to the fact that they investigated systems with (in our notation) $s \geqslant 1.5$, which are not displacive enough to exhibit classical behaviour for short-range coupling.

7. Summary

We have analysed the Ginzburg interval (GI) in soft-mode phase transitions using the rigid unit mode (RUM) picture. This applies to framework structures of relatively stiff units linked by shared corner atoms, and to 'cogwheel' structures where the rotations and/or
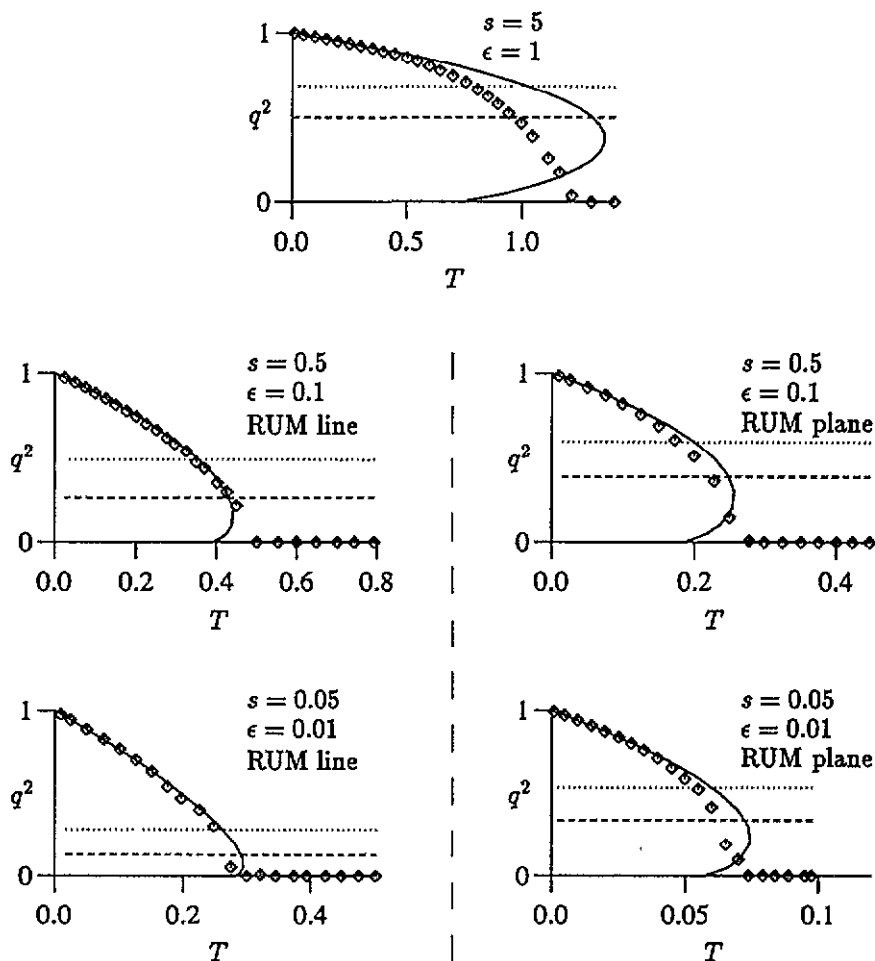
Figure 5. The analogue of figure 4, for the second model parameter series from (52).

displacements of units touching one another are linked due to steric hindrance. The essential features of RUM systems are displaciveness, i.e. closeness to the soft-mode limit ($s \ll 1$) and anisotropy ($\epsilon \ll 1$) or, equivalently, the presence of two very different correlation length scales. We have found that the magnitude of the GI relative to the transition temperature can in principle have any value, from large to very small. The actual value depends on the balance of s and ϵ as well as on the dimensionality of the RUM sector in k-space; in particular, in the limit of infinitely rigid structural units, the GI is zero for a system with a RUM line but finite for the case of a RUM plane.

The results of the theoretical analysis were found to agree with the results of computer simulations and experimental observations on the framework perovskites $SrTiO_3$ and $LaAlO_3$ and the cogwheel structure K_2SeO_4. Qualitative estimates of the model parameters and the size of the GI for framework silicates were also given, using quartz and cristobalite as examples. We found in all these cases a GI ΔT_G of the order of $0.1T_c$ or less, a value which is, as expected, considerably smaller than in typical order–disorder phase transitions (see for example [8]).

In conclusion, it is worth emphasizing that although the inherent anisotropy of RUM systems can in principle lead to a large GI, this effect is countered by the fact that almost all the real materials that we have considered are very displacive, i.e. close to the soft-mode limit, leading to a fairly small GI. Further investigation is needed to clarify the extent to which this reflects the behaviour of real materials in general.

Appendix 1. Results of the IM approximation

In this appendix we summarize the results of the IM (independent-mode) approximation as applied to our model effective Hamiltonian for RUM systems (28). For more details on the IM approximation, we refer the reader to [8, 15]. We emphasize that all results are obtained from classical statistical mechanics without taking quantum mechanical corrections into account.

The IM approximation considers the class of 'trial Hamiltonians' that are quadratic in the deviations of the ϕ_i from their mean values $\bar{\phi}_i \equiv \langle \phi_i \rangle$:

$$\Delta\phi_i = \phi_i - \bar{\phi}_i. \tag{A1.1}$$

These 'trial Hamiltonians' can be written in the form

$$H^{\mathrm{IM}} = \frac{1}{2} \sum_k K(k) |\Delta\phi(k)|^2 \tag{A1.2}$$

and thus decouple the different Fourier modes $\Delta\phi(k)$ of the system, treating their fluctuations as independent. Since we have set the mass scale to unity, we can identify the $K(k)$ with the renormalized frequencies (within the IM approximation) of the corresponding phonon modes:

$$K(k) \equiv \omega_{\mathrm{ren}}^2(k). \tag{A1.3}$$

By minimizing a 'trial free energy' which is an upper bound for the true free energy, the IM approximation establishes the trial Hamiltonian that best approximates the behaviour of a system described by the exact Hamiltonian (28).

Assuming as in our model that $J(k)$ has its minimum at $k = 0$, the ordered (low-temperature) phase is uniform and can be characterized by an order parameter Q such that

$$\bar{\phi}_i = Q = \frac{1}{N} \sum_j \bar{\phi}_j = \frac{1}{\sqrt{N}} \langle \phi(0) \rangle. \tag{A1.4}$$

If we further use the fact that for $J(k)$ as defined in (25) and (26) we have $J(0) = 0$, the results of the IM approximation can be written as follows.

In the ordered phase ($Q \neq 0$)

$$K(k) = J(k) + 2sJq^2 \tag{A1.5}$$

where $q = Q/Q_0$ is the order parameter normalized to its zero-temperature value given by $Q_0^2 = sJ/B$. The value of q as a function of temperature is determined as the solution of the equation

$$1 - q^2 = (T/T_c^{\mathrm{IM}})c(q^2) \tag{A1.6}$$

where

$$c(q^2) = \frac{1}{N} \sum_k \frac{J^{\text{IM}}}{J(k) + 2sJq^2} \tag{A1.7}$$

is a decreasing function of its argument with

$$c(0) = 1 \tag{A1.8}$$

and we have further used the definitions

$$3k_B T_c^{\text{IM}} = J^{\text{IM}} Q_0^2 \qquad \frac{1}{J^{\text{IM}}} = \frac{1}{N} \sum_k \frac{1}{J(k)}. \tag{A1.9}$$

Here T_c^{IM} is the lower stability limit of the disordered phase within the IM approximation; however, the equation of state (A1.6) admits stable, or at least metastable, solutions with non-zero Q up to a temperature $T_+^{\text{IM}} > T_c^{\text{IM}}$, and the IM approximation actually predicts a first-order transition at a temperature between T_c^{IM} and T_+^{IM}, where the free energies of ordered and disordered phase become equal.

In the disordered phase ($Q = 0$), $K(k)$ has to be obtained self-consistently from

$$K(k) = -sJ + J(k) + 3sJ\Delta^2/Q_0^2 \tag{A1.10}$$

where

$$\Delta^2 = \frac{1}{N} \sum_i \langle (\Delta\phi_i)^2 \rangle = k_B T \frac{1}{N} \sum_k (K(k))^{-1} \tag{A1.11}$$

measures the local fluctuation of the fields ϕ_i.

We remark that the IM approximation predicts a temperature-dependent shift of the phonon spectrum that is uniform across the Brillouin zone, since the difference between the squared renormalized frequencies, $K(k)$, and the squared bare frequencies, $-sJ + J(k)$, is independent of k in the ordered phase (A1.5) as well as in the disordered phase (A1.10). The scale of this frequency shift is set by $sJ = A$, as can be seen from (A1.5), (A1.10) using the fact that q^2 and Δ^2/Q_0^2 are both of order unity or less.

Appendix 2. Limits of validity of the IM approximation

In order to calculate the size of the GI, we now want to establish a criterion for validity of the IM approximation when applied to the effective Hamiltonian (28). As discussed in sections 3 and 4, the limit of validity of the IM approximation determines the size of the GI since the IM is the best classical approximation available for the effective Hamiltonian (28) in the displacive regime that we are interested in. According to our general remarks in section 3, we restrict our attention to the validity of the IM approximation in the ordered (low-temperature) phase.

We determine the limits of validity of the IM approximation by checking its consistency with the exact relationship between the susceptibility of the local order parameter $\bar{\phi}_i$ to a linearly coupled external field, and the fluctuations of the ϕ_i. We denote the external field at site j by h_j and define the susceptibility as

$$\chi_{ij} = \partial\bar{\phi}_i/\partial h_j. \tag{A2.1}$$

In Fourier space, the exact relation between this susceptibility and the fluctuations of the ϕ_i is then

$$\chi(k) = \frac{1}{k_\mathrm{B}T} \langle |\Delta\phi(k)|^2 \rangle \tag{A2.2}$$

where we have used the definition

$$\chi_{ij} = \frac{1}{N} \sum_k \chi(k) \exp[ik \cdot (r_i - r_j)] \tag{A2.3}$$

for the Fourier transform of the susceptibility. The right-hand side of (A2.2) is, from the simple form of the IM Hamiltonian (A1.2), simply equal to $1/K(k)$. The left-hand side can be evaluated by introducing the coupling term $-\sum_i h_i\phi_i$ into the original Hamiltonian (28) and then calculating the $\bar{\phi}_i$ for infinitesimal fields h_i within the IM approximation. One obtains [15, 16] as the analogues of (A1.5), (A1.6)

$$K(k) = -sJ + J(k) + 3sJ(\bar{\phi}^2 + \Delta^2)/Q_0^2 \tag{A2.4}$$

with $\bar{\phi}^2 = (1/N) \sum_i \bar{\phi}_i^2$, and

$$sJ(3\Delta^2/Q_0^2 - 1)\bar{\phi}_i + sJ\bar{\phi}_i^3/Q_0^2 + \sum_j J_{ij}\bar{\phi}_j = h_i. \tag{A2.5}$$

In writing these equations we have used the Fourier transform J_{ij} of $J(k)$ defined in a way exactly analogous to (A2.3).

By taking the derivative of (A2.5) with respect to the external field h_j and afterwards setting all external fields to zero, one can derive that in the ordered phase

$$\left(\chi(k)\right)^{-1} = K(k) + \delta(k)6sJq^2\frac{\mathrm{d}\Delta^2}{\mathrm{d}\bar{\phi}^2} \tag{A2.6}$$

where from the definition (A1.11) of Δ^2 and (A2.4), one has

$$\Delta^2 = \frac{k_\mathrm{B}T}{N} \sum_k \frac{1}{-sJ + J(k) + 3sJ(\Delta^2 + \bar{\phi}^2)/Q_0^2} \tag{A2.7}$$

which implicitly defines Δ^2 as a function of $\bar{\phi}^2$. From (A2.6), one sees that the exact fluctuation-susceptibility relation (A2.2) is satisfied for all wavevectors $k \neq 0$, but that in order for it to hold also for $k = 0$, we require

$$\left|\frac{\mathrm{d}\Delta^2}{\mathrm{d}\bar{\phi}^2}\right| \ll \frac{K(0)}{6sJq^2} = \tfrac{1}{3}. \tag{A2.8}$$

The derivative can be evaluated to be

$$\frac{\mathrm{d}\Delta^2}{\mathrm{d}\bar{\phi}^2} = -\frac{z}{1+z} \tag{A2.9}$$

where z is given by

$$z = \frac{sJ}{Q_0^2} \frac{3k_\mathrm{B}T}{N} \sum_k \frac{1}{\left(J(k) + 2sJq^2\right)^2}. \tag{A2.10}$$

The inequality (A2.8) is therefore $z/(1 + z) \ll \frac{1}{3}$ or, equivalently, $z \ll \frac{1}{3}$, yielding the criterion

$$\frac{3}{4} \frac{T}{T_c^{IM}} \frac{J^{IM}}{sJ} \frac{1}{N} \sum_k \frac{1}{\left(q^2 + J(k)/2sJ\right)^2} \ll 1 \tag{A2.11}$$

for consistency of the IM approximation with the fluctuation-susceptibility relation (A2.2). In our approach to establishing the limits of validity of the IM approximation, the lower boundary of the GI is then determined by setting the left-hand side of the last inequality equal to a constant of the order of unity and solving for $q^2 = q_G^2$, the square of the normalized order parameter at the lower boundary of the GI.

References

[1]   Berge B, Bachheimer J P, Dolino G, Vallade M and Zeyen C M E 1986 *Ferroelectrics* **66** 73
[2]   Vallade M, Berge B and Dolino G 1992 *J. Physique* I **2** 1481
[3]   Dove M T, Giddy A P and Heine V 1993 *Trans. Am. Cryst. Assoc.* **27** 65
[4]   Dove M T, Giddy A P and Heine V 1992 *Ferroelectrics* **136** 33
[5]   Salje E K H 1990 *Phase Transitions in Ferroelastic and Coelastic Crystals* (Cambridge: Cambridge University Press)
[6]   Ginzburg V L 1960 *Sov. Phys.–Solid State* **2** 1824
[7]   Kadanoff L P, Götze W, Hamblen D, Hecht R, Lewis E A S, Palcianskas V V, Rayl M and Swift J 1967 *Rev. Mod. Phys.* **39** 395
[8]   Bruce A D 1980 *Adv. Phys.* **29** 111
[9]   Levanjuk A P 1959 *Sov. Phys.–JETP* **9** 571
[10]   Amit D J 1974 *J. Phys. C: Solid State Phys.* **7** 3369
[11]   Giddy A P, Dove M T, Pawley G S and Heine V 1993 *Acta Crystallogr.* A **49** 697
[12]   Heine V, Chen X, Dattagupta S, Dove M T, Evans A, Giddy A P, Marais S, Padlewski S, Salje E and Tautz F S 1992 *Ferroelectrics* **128** 255
[13]   Tautz F S, Heine V, Dove M T and Chen X 1991 *Phys. Chem. Minerals* **18** 1991
[14]   Giddy A P 1991 *PhD Thesis* University of Cambridge
[15]   Eisenriegler E 1974 *Phys. Rev.* B **9** 1029
[16]   Sollich P 1992 *MPhil Thesis* University of Cambridge
[17]   Mueller K A and Berlinger W 1971 *Phys. Rev. Lett.* **26** 13
[18]   Cowley R A 1980 *Adv. Phys.* **29** 1
[19]   Stirling W G 1972 *J. Phys. C: Solid State Phys.* **5** 2711
[20]   *Landolt–Börnstein New Series* 1976 *Numerical Data and Functional Relationships in Science and Technology* Group III, vol 7e (Berlin: Springer)
[21]   Cowley R A, Buyers W J L and Dolino G 1969 *Solid State Commun.* **7** 181
[22]   Ginzburg V L, Levanjuk A P and Sobyanin A A 1987 *Ferroelectrics* **73** 171
[23]   Kjems J K, Shirane G, Mueller K A and Scheel H J 1973 *Phys. Rev.* B **8** 1119
[24]   Galasso F S 1969 *Structure, Properties and Preparation of Perovskite-Type Compounds* (Oxford: Pergamon)
[25]   Etxebarria I, Perez-Mato J M and Criado A 1990 *Phys. Rev.* B **42** 8482
[26]   Iizumi M, Axe J D, Shirane G and Shimaoka K 1977 *Phys. Rev.* B **15** 4392
[27]   Etxebarria I, Perez-Mato J M and Madariaga G 1992 *Phys. Rev.* B **46** 2764
[28]   Etxebarria I, Lynden-Bell R M and Perez-Mato J M 1992 *Phys. Rev.* B **46** 13687
[29]   Chen Z Y 1990 *Phys. Rev.* B **41** 9516
[30]   Dolino G, Berge B, Vallade M and Moussa F 1992 *J. Physique* I **2** 1461
[31]   Schmahl W W, Swainson I P, Dove M T and Graeme-Barber A 1992 *Z. Kristallogr.* **201** 125
[32]   Sanders M J, Leslie M and Catlow C R A 1984 *Chem. Commun.* **1984** 1271
[33]   Swainson I P and Dove M T 1993 *Phys. Rev. Lett.* **71** 193
[34]   Schneider T and Stoll E 1976 *Phys. Rev.* B **13** 1216
[35]   Schneider T and Stoll E 1978 *Phys. Rev.* B **17** 1302
[36]   Kerr W C and Bishop A R 1986 *Phys. Rev.* B **34** 6295
[37]   Padlewski S, Evans A K, Ayling C and Heine V 1992 *J. Phys.: Condens. Matter* **4** 4895
[38]   Dove M 1988 *Physical Properties and Thermodynamic Behaviour of Minerals (NATO ASI Series 225)* ed E K H Salje (Dordrecht: Riedel) pp 501–90
[39]   Allen M P and Tildesley D J 1987 *Computer Simulation of Liquids* (Oxford: Oxford University Press)